Renewable Energy 170 (2021) 1308–1323

Contents lists available at ScienceDirect

Renewable Energy

journal homepage: www.elsevier.com/locate/renene

A standardised tidal-stream power curve, optimised for the global resource

Matt Lewis [a, *], Rory O'Hara Murray [b], Sam Fredriksson [c], John Maskell [d], Anton de Fockert [e], Simon P Neill [a], Peter E Robins [a]

[a] School of Ocean Sciences, Bangor University, UK
[b] Marine Scotland Science, The Scottish Government, UK
[c] University of Gothenburg, Swedish Meteorological and Hydrological Institute, Sweden
[d] JM Coastal Ltd, UK
[e] Deltares, Delft, the Netherlands

ARTICLE INFO

Article history:
Received 29 November 2020
Received in revised form
3 February 2021
Accepted 6 February 2021
Available online 15 February 2021

Keywords:
Tidal-stream energy
Power curve
Resource
Optimisation
Renewable energy

ABSTRACT

Tidal-stream energy resource can be predicted deterministically, provided tidal harmonics and turbine-device characteristics are known. Many turbine designs exist, all having different characteristics (e.g. rated speed), which creates uncertainty in resource assessment or renewable energy system-design decision-making. A standardised normalised tidal-stream power-density curve was parameterised with data from 14 operational horizontal-axis turbines (e.g. mean cut-in speed was ~30% of rated speed). Applying FES2014 global tidal data (1/16° gridded resolution) up to 25 km from the coast, allowed optimal turbine rated speed assessment. Maximum yield was found for turbine rated speed ~97% of maximum current speed (maxU) using the 4 largest tidal constituents (M2, S2, K1 and O1) and ~87% maxU for a "high yield" scenario (highest Capacity Factor in top 5% of yield cases); with little spatial variability found for either. Optimisation for firm power (highest Capacity Factor with power gaps less than 2 h), which is important for problematic or expensive energy-storage cases (e.g. off-grid), turbine rated speed of ~56% maxU was found – but with spatial variability due to tidal form and maximum current speed. We find optimisation and convergent design is possible, and our standardised power curve should help future research in resource and environmental impact assessment.

1. Introduction

Tidal energy can be extracted using hydrokinetic devices or "in-stream" tidal-stream energy converters (e.g. Refs. [1,2]), based on the principle that power (P) is a function of the cube of the volumetrically averaged current velocity (u) over the rotor swept area (A), turbine power coefficient (Cp) and seawater density (ρ):

$$P = \frac{1}{2}\,\rho\, Cp\, A\, u^3. \quad (1)$$

As nations look to increase their renewable energy capacity in response to climate change [3] or improve access to affordable electricity [4,5], tidal-stream energy could offer one substantial renewable resource due to the predictability and reported power quality [6]. Three main types of tidal-stream turbines are in various stages of development (for a review, see Ref. [7]): (1) horizontal axis turbines; (2) vertical axis turbines; and (3) rotating and reciprocating devices. This paper shall focus on the horizontal axis turbine, used for the majority of test and operational deployments; hence much data is available to inform and constrain our analysis – such as estimation of device efficiency and the device power coefficient (Cp: extracted power relative to the available power), alongside turbine behaviour parameters including turbine cut-in and rated speed (see Refs. [8,9]).

The potential of tidal-stream energy for a sustainable future is immense (~2.5 TW M2 tidal energy is dissipated globally – see Ref. [10]), with diverse applications: from predictable contributions of renewable electricity to a national grid [3], to energy solutions for remote communities and industries (e.g. Ref. [11]) such as contributing to UN sustainability goals and reducing energy poverty (e.g. Ref. [12]). However, the high costs associated with tidal energy (e.g. Ref. [13]) need to be reduced for the true potential

* Corresponding author.
E-mail address: m.j.lewis@bangor.ac.uk (M. Lewis).

https://doi.org/10.1016/j.renene.2021.02.032

of tidal energy to be realised; such as cost reduction through economies of scale (e.g. Ref. [14], and deployment constraints (e.g. Ref. [15]). As power is proportional to the cube of tidal current, industry has predominately focused on turbines with high rated speed (>2.5 m/s) at so-called "first generation sites" [15]. It is unclear if mass-produced lower resource tidal-stream turbines for "high-value markets" could provide another route to cost reduction for the industry, but the motivation for this study.

As discussed in the US Dept. Energy "Powering the Blue Economy" [16], there is a diverse range of potential power demands (e.g. both in size and timing of power required) and higher value markets (thus economic viability). We hypothesise that previous focus on MegaWatt-scale contributions from tidal-stream turbines (with high rated speeds above 2.5 m/s) is creating uncertainty and may not be suitable for all potential renewable energy markets [16]. For example, there has been a reported need for power curves to aid resource mapping studies with one (1 m/s cut-in and 2.7 m/s rated) predominately being applied tidal turbine design (e.g. Refs. [17–19]) which may introduce bias in resource assessment [20]. Furthermore, Robins et al. [19] proposed that turbines suitable for lower flows would reduce temporal variability to the resource and increase resultant net power. Tidal-stream energy resource therefore appears uncertain, in part, due to uncertainty of end-user power needs and device design.

Mapping the tidal resource for a region relies on validated hydrodynamic models, which numerically solve versions of the Navier-Stokes equations to fully capture tidal dynamics. Theoretical resource estimates for a region calculate tidal power from the ocean model output variables to be applied in equation (1). Tidal resource has been shown to be affected by the power extracted (e.g. Refs. [21–23]), hence technical resource assessment often explicitly include power extraction of tidal turbines to further improve potential yield estimates (e.g. Refs. [24,25]). Environmental impact assessments to the deployment of tidal turbines also require power extraction to be explicitly resolved in the ocean model simulations; for example, impacts to circulation and associated processes (e.g. Ref. [26]), sediment transport pathways [27] and morphodynamics [28].

The drag force (Fd) of a tidal turbine is represented within hydrodynamic model simulations applying equation (1) as:

$$Fd = \frac{p}{u}; \tag{2}$$

hence the impact of tidal energy conversion can be explicitly resolved in environmental impact and resource assessments (see Ref. [23]). Tidal-stream turbine behaviour is predominately based on first generation technologies [15]; where cut-in speed (Vs), and rated speed (Vr: the current speed where maximum or "rated power" (Pr) is extracted, with power "capped" or "shed" for current speeds above Vr) – must be resolved to adequately represent turbine behaviour (e.g. Ref. [25]). First generation tidal-stream turbines are defined by Lewis et al. [15] as having a rated speed ~2.5 m/s, and, whilst many devices indeed have high rated speeds, a number of lower flow devices (e.g. Kites – see Ref. [29]) and applications [30] have been discussed. Indeed, in many resource assessments, power curve information has been stated as necessary for future work (e.g. Refs. [13,15,31]).

The lack of data to parameterise turbine behaviour presents a significant challenge due to uncertainty in the parameterisation of tidal-stream turbine behaviour. The impact of various tidal turbine power curves to the technical resource assessment is shown in Fig. 1; where a 15-day time-series of two harmonics (M2 amplitude of 2 m/s and S2 amplitude of 0.5 m/s) is applied to estimate theoretical power density (P/A using Eq. (1)), and the theoretical power curve of two devices: $Vr = 2.5$ m/s and $Vs = 1$ m/s (from Ref. [15]), and $Vr = 2$ m/s and $Vs = 0.5$ m/s (from Ref. [32]). Although rated turbine speed (Vr) differs by 0.5 m/s between the two devices of Fig. 1, with mean power and mean daily energy difference of 18% and 23% respectively, the maximum drag (thus impact, estimated from Eq. (2)) differed by 41%. Moreover, the Capacity Factor (CF), defined here as the ratio of energy converted relative to the maximum energy that could be converted (i.e. if at rated power throughout the time-series), varied by 14% between the two devices of Fig. 1; with a 19% difference in the time of zero power (so called downtime) and a 2 h difference in the longest duration window of zero power output, which has implications for storage design and whole system costs.

Given that tides are almost entirely deterministic (e.g. Ref. [6]), and the wide variety of potential markets globally (from large-scale power contributions to national electricity distribution networks to remote "off-grid" industries and communities): are the present range of tidal-stream turbine designs suitable for all global markets, and can a scalable convergent solution be found? This paper aims to firstly consolidate the diverse range of horizontal axis tidal turbines to a scalable power curve for unbiased resource and impact assessments. The standardised power-density curve can then be applied to explore convergence based on the global tidal-stream resource. We do not include the swept area in our analysis as this is likely to be based on local bathymetric constraints, life cycle assessment and cost optimisation. Instead our objective is to establish a method, which can be applied in the future to include cost optimisation based on future markets and mass-production principles [14,33]: providing a constructive step towards a resource-led globally-optimal engineering solution for the renewable energy industry.

2. Method

This study is composed of three parts: firstly, power curve data is compiled for the majority of published horizontal tidal-stream turbines (i.e. all that could be found). Rated power (Pr) and flow speed (Vr) allow the power coefficient (Cp) and thrust coefficient (Ct) to be estimated, using variables from equations (1) and (2), because:

$$Ct = \frac{2\,F}{\rho\,A\,u^2}\,; \tag{3}$$

$$Cp = \frac{2\,P}{A\,\rho\,u^3}. \tag{4}$$

Consolidating the data, a normalised theoretical mean power density curve relative to rated power (i.e. P/Pr and u/Vr) can be established (i.e. swept area removed), and also compared to observed variability in a grid-connected tidal-stream turbine (published in Ref. [6]). Here, density of seawater (ρ) is assumed to be 1027 kg/m∧3 and the turbine is operated at constant Tip Speed Ratio (TSR) irrespective of swept area (A) or flow speed (u): i.e. that Cp does not vary with flow speed and Tip Speed Ratio [8,9].

The second part of our method will apply the average power density curve information (which we call the normalised power curve) to resolve optimal power curve characteristics for the diverse range of potential markets and tidal energy sites globally:

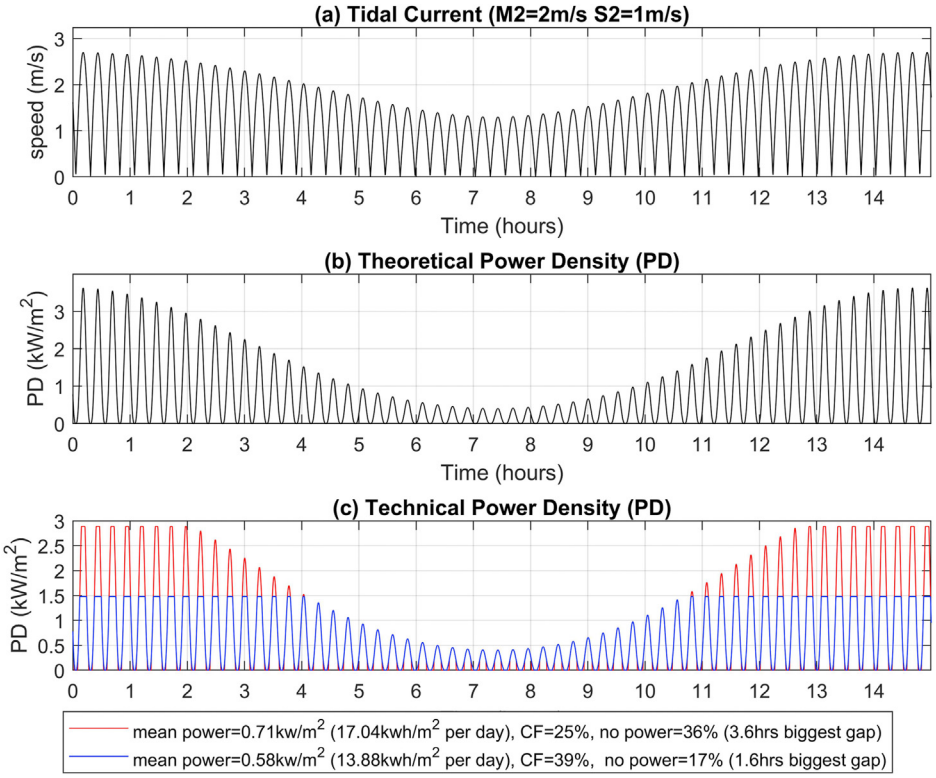

Fig. 1. A demonstration of the effect of two tidal power curves on resource assessment. A spring-neap time-series (2 m/s M2 Cmax and 0.5 m/s S2 Cmax) of tidal current speed (panel a) is converted to theoretical power density (PD) in panel b and technical power density (panel c) for a power curve rated at 2.5 m/s (red line) and 2.0 m/s (blue line).

for example, does the optimal power curve for a remote island/industry differ to an optimal tidal power curve for electricity supply to a grid?

Depth averaged tidal current information was based on the FES2014 dataset (Finite Element Solution data assimilated global tide model), which has a global grid resolution of 1/16° [34]. The FES2014 dataset was masked using the NASA distance-to-coast dataset (resolution 1/25°) which was created using the Generic Mapping Tools (GMT) coastline. Global tidal data of the four principal semi-diurnal and diurnal tidal constituents (M2, S2, K1, O1), between latitudes 70°S and 70°N and included only ocean grid cells that were within 25 km from land were extracted. We assume tidal energy development beyond 25 km is not economically feasible based on challenges with connecting to shore, and have removed tidal analysis from high latitude (>70°) due to ice interaction challenges and uncertainties.

Applying the normalised power curve to a wide range of rated speeds (*Vr* discretised in 0.1 m/s bins between 0.3 m/s and 6 m/s) allows power density curves for all potential tidal-stream turbines to be applied to one year tidal current time-series (5 min frequency). The tidal current time-series at each location was calculated using the "t_tide" toolbox: a harmonic tidal prediction method, where a time-series is described from the sum of sinusoids at frequencies specified from astronomical parameters [35]. Global tidal harmonics data were used from the FES2014 product [34,36] for all resolved coastal locations (<25 km from land). An optimal power density curve was selected for each site using three scenarios (A, A2 and B) to represent the diversity of end user needs; from weighting the optimal tidal turbine power density curve based on firm and constant power, or maximum possible yield. Hence, the range between high yield and firm power (scenarios A and B) should therefore represent all potential optimal tidal turbine solutions; providing a sensitivity test to power curve choice in resource assessment, but also the potential for current technologies and concepts to be scaled for the more globally prevalent, lower flow and power demand markets.

Scenario A (maximum yield): the power density curve that gave the highest annual energy yield for each site (irrespective of storage and end user needs). We assume such a scenario useful in free-market economic systems with national electricity distribution networks.

Scenario A2 (high yield): the highest Capacity Factor (CF) for power density curves that gave the top 5% of annual yields per site. Therefore, although Scenario A2 does not bound the range of potential optimal tidal power curves, it is assumed to represent a likely choice given other resource uncertainties (e.g. higher order tidal harmonic effects, or the impact of waves [15] and weather windows).

Scenario B (Firm yield): the highest yield power density curve that had a maximum gap in power generation below 2 h and consistent peak power (within 2%). We assume such a firm power tidal turbine beneficial for users where likely storage potential is low, or the storage costs are high (for example the use of fly wheels instead of batteries).

The third part of method aims to resolve convergence in an optimal power curve based on the global tidal data; producing simplified rules for industry and researcher to follow (e.g. can we assume tidal turbine rated speed to be equivalent to the peak spring tidal current speed for a given site?) Finally, we investigate the impact of tidal data quality by comparing our 1/16° FES2014

results to that derived from tidal harmonics calculated using a much higher resolution ocean model at 1/100° (~1 km instead of ~7 km spatial resolution) for the UK domain (14°W to 11°E, and 42°N to 62°N). Data were interpolate onto the higher resolution grid and the data of the UK ROMS model details given in Robins et al. [19].

3. Results

Horizontal-axis tidal-stream turbine power density curves were normalised and standardised (Section 3.1), which can be applied to idealised tidal current time-series with increasing complexity in tidal harmonics (Section 3.2), and then applied to global tidal harmonic data (Section 3.3).

3.1. Power curve analysis results

Horizontal axis tidal turbine information was gathered from published data of 14 devices that are in commercial development or deployment (Table 1). We believe data in Table 1 to be the most comprehensive, up-to-date list compiled thus far. We acknowledge that Table 1 is incomplete, with some prototypes and models missing, however convergence of the normalised power-density curve in Fig. 2 is clear – and the addition of devices likely to only impact parameters that are not considered here (e.g. swept diameter mean rated power). Where key variables are missing (noted in Table 1 with *), data were extrapolated using equations (1) and (4).

The rated power density and speed (*Pr* and *Vr* respectively) of the tidal-stream turbines are shown in Fig. 2a, compared to the theoretical (black dash line). Normalised power-density curves of these devices are shown in Fig. 2b, using the mean device power coefficient (*Cp*) of Table 1, assuming *Cp* constant through all flow speeds, alongside the measured power variability (at 0.5 Hz frequency) for a "grid connected" tidal-stream turbine (taken from Ref. [6]). Measured fine-scale power fluctuations of Fig. 2b, likely due to fine-slow flow variability and turbulence (see Ref. [6]), were found to be much larger than variability in mean device characteristics (cut-in and rated speed) for the 14 devices. Therefore Fig. 2 indicates a normalised mean power curve can be used to represent all horizontal axis tidal turbines currently being developed, and apply the power-density curve to global tide data in Section 3.2.

Finally, Fig. 2a shows there is no trend in diameter of the swept rotor area, especially considering the size range of turbines, shown by the large standard deviation in Table 1, hence further justification to use power density in our analysis - as rotor size is likely to depend on local site charactersitics and cost-benefit analysis (which is beyond the scope of this work).

A standardised and normalised power curve for horizontal axis tidal-stream turbines was established using the mean value of Table 1: Cut in speed of the turbine (*Vs*) was found to be 30% of the rated speed (*Vr*) on average with a standard deviation (STD) of 7%, and we assume power coefficient (*Cp*) is constant, at a mean value of 0.37; which allows the power density (*P/A*) to be described relative to the rated power of a device (where *Pr* is expressed as *P/A* relative to the rated, thus between 0% and 100%). It should be noted that the power coefficient (*Cp*) is likely to be affected by a number of variables: flow speed and site turbulence characteristics (including waves), as well as blade design and Tip-Speed-Ratio (see Refs. [8,9]) – however the variability does not significantly affect our results (based on unpublished sensitivity test – varying section 3.2 with *Cp* with one STD: 0.04).

The standardised power curve, based on mean values of Table 1, is shown in Fig. 3a and is described in equation (5), using three conditions:

$$\text{When } Vr > u > 0.3Vr: \; P = \frac{1}{2} 0.37 \, u^3 A;$$

$$\text{when } u < 0.3Vr: P = 0;$$

$$\text{when } u > Vr: \; P = Pr. \tag{5}$$

Moreover, the normalised drag and thrust coefficient (*Ct*) can now also be described (using Equation (2)) – which allows a tidal-stream turbine, unbiased in technology choice, to be represented for future resource and environmental impact assessment hydrodynamic modelling methods. The device agnostic power curve of Fig. 3 therefore only needs a rated power (*Pr*) and swept area (*A*) to be assumed, and we shall explore an optimal *Vr*, based on tidal resource, in Section 3.2.

Table 1
A literature review of 14 horizontal axis tidal-stream turbines, where device characteristics are published or estimated (marked with *), including: rotor diameter (⌀); Rated Power (Pr); power coefficient (*Cp*); cut-in velocity (*Vs*) when the turbine starts to produce power; and rated velocity (*Vr*), the current speed when maximum power (*Pr*) is produced. Labels of devices in Fig. 2 are defined in the ID column.

ID	device	⌀(m)	*Pr* (kW)	*Vr* (m/s)	*Vs* (m/s)	*Vs* (as % of *Vr*)	*Cp**	source
1	MCT		600	*2.5*	*1*	*40*	*0.37*	Lewis et al. [15]
2	Alstrom		1000	*2.7*	*1*	*37*	*0.39*	Lewis et al. [6]
3	sabella D-10		1000	*4*	*1*	*25*	*0.39*	[56]
4	sabella D-15		2300	*4*	*1*	*25*	*0.4*	[56]
5	seagen-S 2 MW twin rotor		1000 (per rotor)	*2.5*	*1*	*40*	*0.4*	[37]
6	Atlantis AR1000		1000	*2.65*	–	–	*0.41*	[37]; Roberts et al. [40]
7	Atlantis AR2000		2000	*3.05*	*<1*	–	*0.36*	Encarnacion et al. [32,37]
8	Verdant gen5		35	*2.59*	–	–	*0.32*	Polygae et al. [57]; Encarnacion et al. [32]
9	Nova		100	*2*	*0.5*	*25*	*0.43*	Encarnacion et al. [32]
10	Voith		1000	*2.9*	–	–	*0.4*	Roberts et al. [40]
11	openhydro		200	*2.5*	–	–	*0.32*	Polygae et al. [57]; Roberts et al. [40]
12	schottel hydro d3		70	*3.7*	*0.9*	*24*	*0.38*	[58]
13	schottel hydro d4		62	*3.1*	*0.8*	*26*	*0.32*	[58]
14	schottel hydro d5		54	*2.6*	*0.7*	*27*	*0.31*	[58]
	Mean	13	816	*2.91*	*0.88*	*30%*	*0.37*	
	Standard Deviation	6	803	*0.6*	*0.18*	*7%*	*0.04*	

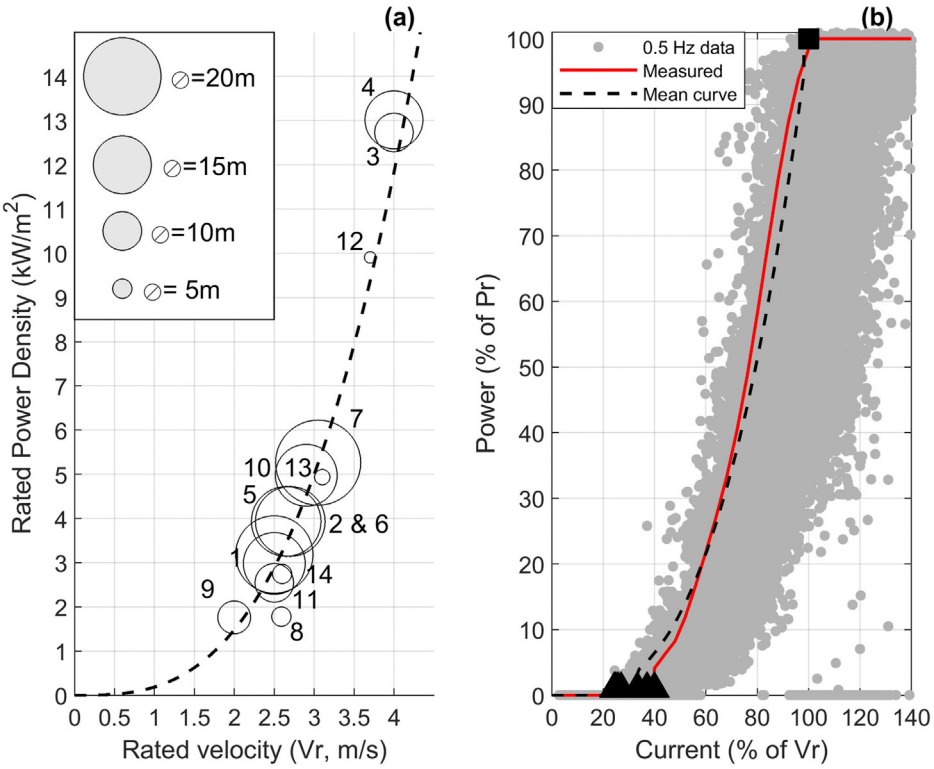

Fig. 2. Tidal-stream turbine characteristics from 14 commercially developed devices (panel a), normalised (relative to rated power and speed) and compared to observed variability (grey dots and averaged power curve in red) from a grid-connected device in Lewis et al. [6].

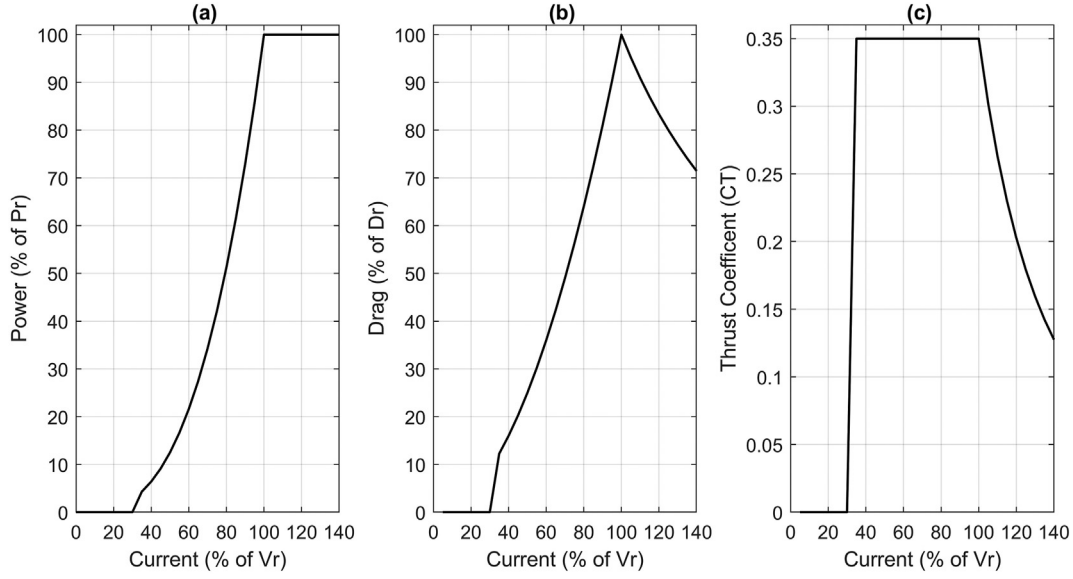

Fig. 3. A standardised power curve, based on 14 horizontal axis tidal-stream turbines, with the associated Drag (as percentage of maximum drag, Dr) and Thrust Coefficient (CT) normalised curves.

3.2. Power density curve optimisation

The standardised normalised power curve of Fig. 3 was applied to a tidal current time-series for a range of rated turbine speeds (*Vr*), with the Capacity Factor (*CF*) and the yield for each theoretical device compared. Capacity Factor (*CF*) was calculated as the percentage of energy captured compared to energy captured if a turbine was at rated speed throughout the timeseries:

$$CF = \frac{\int \frac{1}{2} Cp\, A\, u_t^3}{\int \frac{1}{2} Cp\, A\, Vr^3}). \quad (6)$$

Here, we consider power-density in our analysis, as bathymetry likely to be uncertain in the spatially coarse global data of FES2014

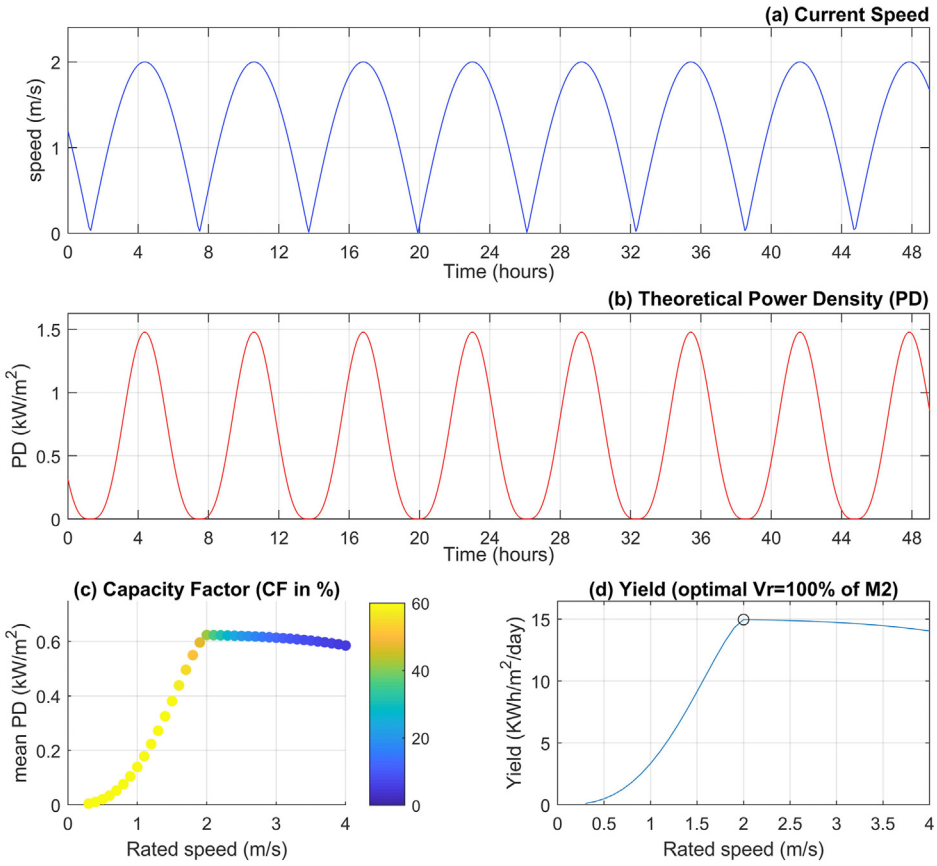

Fig. 4. Single harmonic tidal current (M2 amplitude 2 m/s) over a 2 day period (panel a), and the theoretical power density (PD) of this current (panel b), compared to the mean power density and Capacity Factor (panel c) for multiple tidal-stream turbine power curves, where rated power is capped at rated speed (Vr, and cut-in speed is 30% of Vr), which allows mean daily yield density to be calculated (panel d).

(1/16° see Section 3.3) and we assume swept area (*A* in Eq. (1)) to be controlled by cost and array-design optimisation. Furthermore, the scaling of depth-averaged current (u) to hub-level flow is not included but cannot be represented in global tide data due to sub-scale temporal and spatial variability. The swept area (A) can be removed from our *CF* calculation (of Eq. (6)), as it is a constant in the numerator and denominator integral; therefore our optimisation is independent of swept area, and instead our analysis focuses on the rated speed of a turbine relative to the temporal variability of the tide for a given site.

The mean power density and mean daily yield (kWh/m∧2 per day) were also calculated as metrics of power curve performance for each theoretical power curve at each site. To demonstrate the method, Fig. 4 shows the optimal power density curve (Fig. 3, with rated turbine speeds between 0.3 m/s and 6.0 m/s in 0.1 m/s increments) for an idealised tidal current, with a single M2 (principal lunar semi-diurnal tidal harmonic) of amplitude 2 m/s (hence each peak current is 2 m/s with no variability between tides). The optimal power curve for the simplified case of Fig. 4 is a turbine with a rated speed at 2 m/s (as expected), with an optimal mean power and yield density of ~0.6 kW/m∧2 and 15 kW/m∧2 per day respectively (corresponding *CF* of 41%).

Increasing the complexity of an idealised tide example, we demonstrate the power density optimisation for a site with two harmonics in Fig. 5: M2 and S2 (principal solar semi-diurnal harmonic), which together simulate the fortnightly "spring-neap" cycle that describes 75% of UK tidal variability [19]. Fig. 5 demonstrates the optimal power curve for an extreme case, where the S2 amplitude is 60% of the M2 signal (M2 amplitude = 1 m/s), such that peak current of 1.6 m/s occurs when M2 (period 12.42 h) and S2 (period 12 h) are in-phase (spring tide), and 0.4 m/s peak current speeds occur when M2 and S2 are out-of-phase (neap tide). Optimal yield for Fig. 5 was found when the turbine rated speed was that of the peak spring tide (Vr = 1.6 m/s) but with a much reduced Capacity Factor (17%), due to the extreme nature of the M2/S2 ratio. The importance of weighting the optimal tidal power curve to either yield (i.e. Scenario A or A2) or consistent power (i.e. Scenario B) is demonstrated in Fig. 6.

Variability in choice of an "optimal" power curve, described here as rated turbine speed (Vr) relative to the M2 current amplitude (thus *Vr*/UM2), is demonstrated in Fig. 6 for the range of M2/S2 ratios (M2/S2 of 0 has only an M2 tide, whilst equal M2 and S2 current amplitudes has a ratio of 1), with four metrics of turbine performance that were calculated applying the idealised power density curve of Fig. 3 to a rated turbine speed between 0.3 m/s and 6 m/s (in steps of 0.1 m/s): hence Fig. 6 is independent of resource magnitude. The four metrics of turbine performance in Fig. 6 were based on yield performance relative to the maximum (Capacity Factor in Fig. 6a and yield as a percentage of the maximum possible yield Fig. 6c), and the persistence of power supply: percentage of time no power is produced in Fig. 6b (as opposed to percentage of time at rated power of Fig. 6a) and the largest "power gap" where

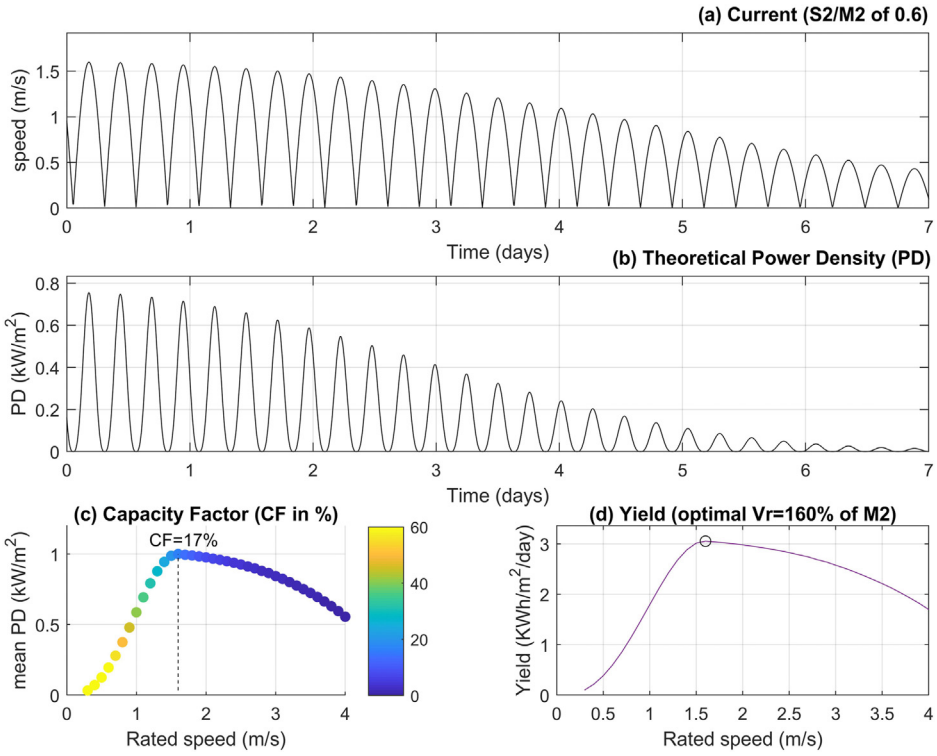

Fig. 5. Spring-Neap tidal current (M2 amplitude 1 m/s, S2 amplitude 0.6 m/s) over a 7 day period (panel a), with the theoretical power density (PD) of this current (panel b). Multiple tidal-stream turbine power curves, where rated power is capped at rated speed (Vr, and cut-in speed is 30% of Vr), are applied to resolve an optimal design using mean power density and Capacity Factor (panel c) and mean daily yield density (panel d).

no power is produced (Fig. 6d). The choice of what an "optimal" tidal-stream turbine is clear at the extremes of the M2/S2 ratio in Fig. 6, where, although extreme, a turbine with a relatively high rated speed would produce large/largest yield but with a low CF and large gaps in power production (thus having consequences in the design and cost of storage and power distribution).

A large number of constituents are needed to describe the complex processes which give realistic tides (hour-to-hour and day-to-day variability in current speed); for example, the K1 and O1 constituents together describe the diurnal inequality (one tide bigger than another in a given day for semi-diurnal tidal systems), which, with the M2 and S2 constituents, can describe tidal form (F value) and thus the diurnal (one tide per day), semi-diurnal (two tides per day) or "mixed" nature of a tide at any site [19]. The complexity of the power curve optimisation, based on resource, is further developed from Fig. 6 by using these four principle constituents (see Fig. 7). Fig. 7 shows theoretical turbine performance for yield (panel a) and persistent power (panel b) for all possible turbine power-density curves (*Vr* 0.3–6 m/s) when varying an idealised tidal current based on the tidal dorm (F value), calculated as the relative magnitude of diurnal and semi-diurnal principle constituents (see Ref. [19]):

$$F\ value = \frac{K1 + O1}{M2 + S2}. \quad (7)$$

Unlike Fig. 6, the result of Fig. 7 was found to be affected by the M2/S2 ratio as multiple combinations of four constituent amplitudes can produce the same F value: Therefore, the result of Fig. 7 is based on a tide with a M2 amplitude of 1 m/s and S2 amplitude being 0.1 m/s (M2/S2 = 0.1). Hence, it should be noted that the result of Fig. 7 would be different if the F value was the same but the M2/S2 ratio were different (based on sensitivity test, an example of which is shown in Appendix Fig. A1). The tidal-stream power density curve optimisation algorithm, which selects the rated speed (*Vr*) for Scenarios A, A2 and B (see Section 2), must therefore be explicitly resolved for each tidal energy site resolve in the global data (Section 3.3). Nevertheless, the uncertainty of optimal rated speed (*Vr*) is clear in Fig. 7 as the divergence of the optimal power-density curve (described as relative rated turbine speed Vr/UM2) for maximum and high yield (Scenario A and A2) or firm power (red line of Scenario B) as the F value increases and the tidal dynamics change from a regular semi-diurnal (F value < 0.25) to a mixed (between 0.25 and 3) or diurnal (F value > 3) system (i.e. one tide per day tide).

3.3. Optimal power curve analysis for the world

Spatial variability of tidal dynamics are shown in Appendix Figure A2 as details from data are not clear. The variability of global tidal dynamics is shown in Fig. 8 relative to resource, calculated here as maximum tidal current speed (maxU) using the sum of the four major tidal dynamics M2, S2, K1 and O1. Probability exceedance (Prob Exc.) of resource (maxU) resolved in FES2014 data up to 25 km from a land mass is shown in Fig. 8a; ~12.8% of sites have maxU>1 m/s, 3.6% of sites have maxU>1.5 m/s, ~1.1% sites have maxU>2 m/s and ~0.3% of global sites resolved have maxU>2.5 m/s. The majority of sites have a dominant M2 current amplitude ~70% of maxU; however some potential tidal energy sites (e.g. maxU>2 m/s) have a much lower M2 contribution (see Fig. 8b),

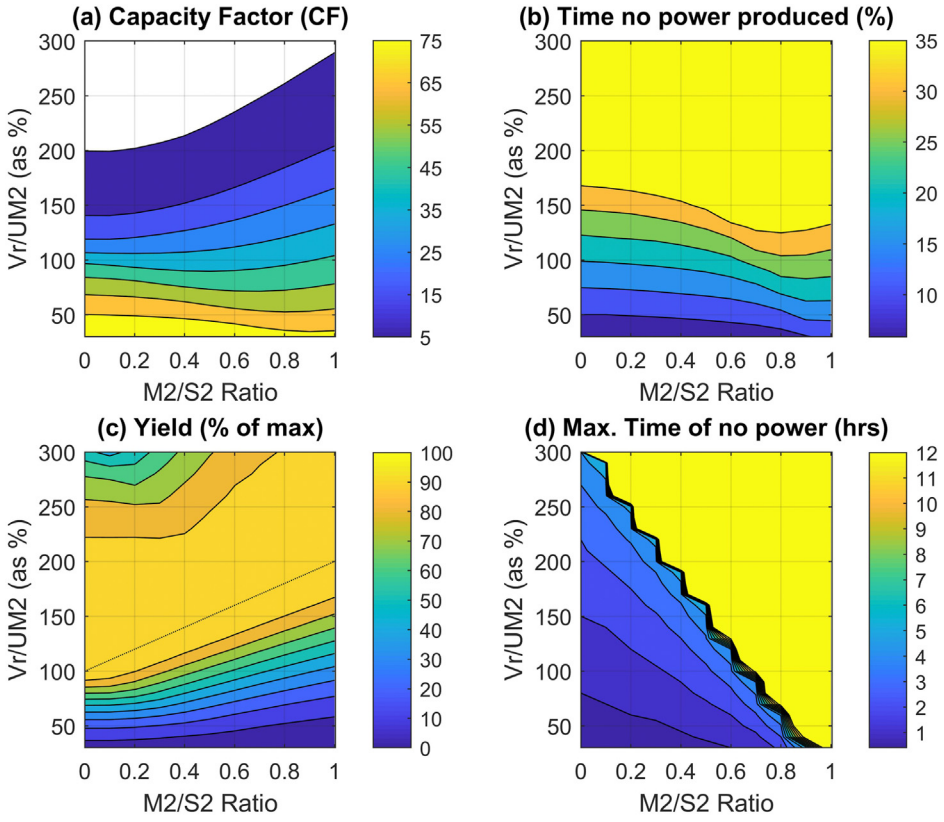

Fig. 6. Performance of multiple tidal-stream power curves, represented here as rated speed (*Vr*) relative to the resource (amplitude of M2 harmonic: *UM2*), for a given site where the tidal currents are controlled solely by the spring-neap cycle and the ratio of M2 and S2 amplitude (M2/S2 of 0 has only an M2 tide, whilst equal M2 and S2 current amplitudes has a ratio of 1). Turbine performance is described using Capacity Factor (a), percentage of time no power produced (b), (c) mean yield density (relative to maximum possible) and (d) the longest period of zero power in a 15 day time-series.

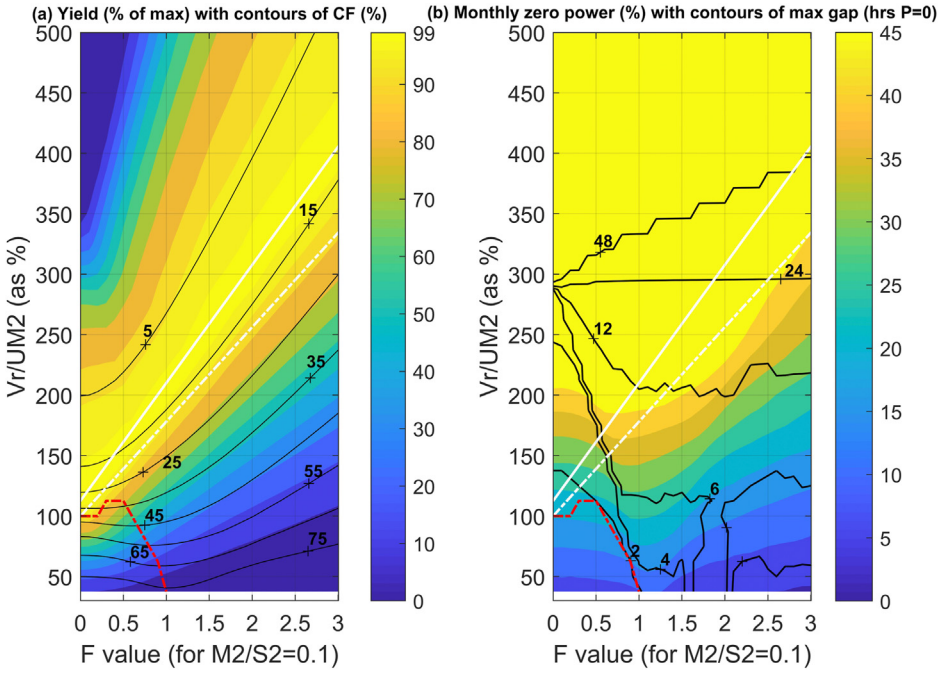

Fig. 7. Tide currents harmonic characteristic tidal form (F value), rated turbine speed (relative to M2 current amplitude UM2) and subsequent yield and Capacity Factor (CF) shown in panel a, with mean monthly percentage of zero power and maximum period of no power (max gap) in panel b. Lines of optimal power curve shown in solid white for selection of maximum yield (Scenario A), high yield (scenario A2) as dashed white line and firm power (power gap < 2 h with highest CF: scenario B) as red dashed line.

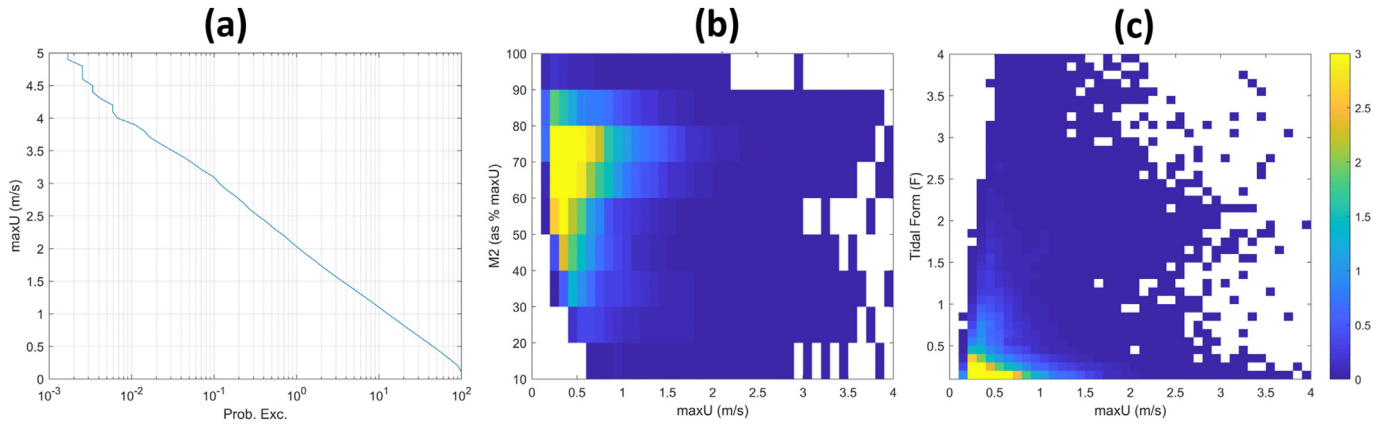

Fig. 8. Global variability of tidal dynamics, described as maximum flow (maxU) percentage exceedance (a) for sites "coastally" (<25 km offshore) resolved in the FES2014 data, (b) coloured percentage occurrence of M2 amplitude contribution to the maximum flow (as percentage of M2 current amplitude compared to maximum current speed), and (c) coloured percentage occurrence of the tidal form (F value) that describes the diurnal (F > 3) to semi-diurnal (F < 0.25) nature of the tide.

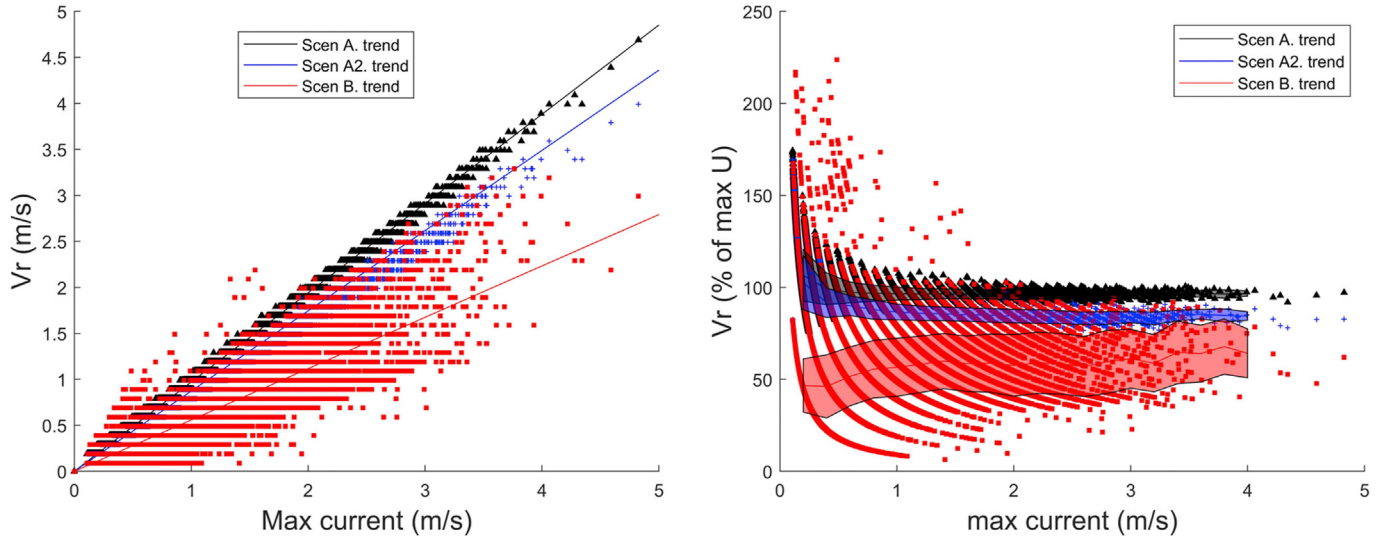

Fig. 9. Rated tidal-stream turbine speed using standardised power density curve and three optimal solutions: Scenario A (maximum yield density shown in black), Scenario A2 (high yield density shown in blue) and Scenario B (firm power shown in red).

Table 2
Optimal rated tidal-stream turbine speed (*Vr*) relative to maximum tidal current speed (MaxU) at any given "coastal" site globally for three optimal power scenarios, with two methods of representing Vr: absolute with linear regression of max U and Vr (with linear regression score: RSQ), and Vr relative to maxU at site, discretised into 0.5 m/s groups with mean Vr (as % maxU) and associated standard deviation (std), with the Pearson correlation score (RHO) is given to indicate strength of statistical fit at 5% confidence.

		Optimal *Vr* scenario:		
		Max yield (scenario A)	High yield (scenario A2)	Firm power (scenario B)
Absolute *Vr* trend	RSQ	~100%	~100%	92%
	trend	$Vr = 0.97*maxU$	$Vr = 0.87*maxU$	$Vr = 0.56*maxU$
Mean *Vr* (as % of maxU) with standard deviation in brackets (std)	maxU	*Vr* as % of maxU (std)		
	0.5 m/s	107 (17)	102 (17)	49 (13)
	1.0 m/s	99 (8)	93 (9)	48 (17)
	1.5 m/s	97 (4)	87 (4)	57 (16)
	2.0 m/s	96 (3)	86 (4)	59 (15)
	2.5 m/s	96 (2)	85 (4)	58 (16)
	3.0 m/s	96 (2)	84 (3)	58 (16)
	3.5 m/s	96 (2)	84 (3)	60 (17)
	4.0 m/s	96 (2)	85 (3)	64 (16)
	4.5 m/s	96 (2)	84 (3)	67 (12)
	RHO	−0.28	−0.43	0.24

which can also be seen in Fig. 8c. Grouping the tidal data of Fig. 8c: 53% of sites resolved had F value below 0.25 (semi-diurnal tides) and 46% were "partial" (F value between 0.25 and 3), with relatively large contributions of K1 and O1 constituents. Some "high tidal resource" (e.g. maxU>3 m/s) of Fig. 8c exhibit F values above 3 (one tide per day), but account for ~1% of the sites resolved. Fig. 8 therefore indicates tidal dynamics at potential tidal-stream energy sites, and thus the temporal variability of resource, will vary greatly around the world, and any analysis that considers low flow sites (e.g. maxU<2.5 m/s) will have an exponentially greater number of sites with varying tidal dynamics to consider (see Fig. 7).

Applying the standardised power curve method (see Section 2), the optimal rated turbine seed (*Vr*) for Scenarios A, A2 and B were computed (e.g. shown for an idealised tide in Fig. 7), and are shown in Fig. 9. Optimal rated tidal-stream turbine speed (*Vr*) using global data is shown in Fig. 9 as absolute (Fig. 9a) and as a percentage of annual maximum tidal current speed (Fig. 9b). Both maximum (scenario A) and high (scenario A2) optimisation solutions showed little variability with the exception of low resource sites (where maximum current speed was below 1 m/s), with a good linear regression fit (panel a) and small standard deviation (shaded region of panel b) of Fig. 9 (values given in Table 2). Optimal *Vr* for Scenario B (firm power) had a large amount of variability and some trend apparent with tidal resource (Table 2 and Fig. 9), likely because the result was greatly affected by tidal form (i.e. the relative contribution of diurnal constituents K1 and O1).

Annual maximum current speed (maxU) was based on the peak current speed simulated at a given site in 2020 using the sum of four tidal constituent amplitudes (e.g. UM2), calculated the major axis length of each tidal constituent ellipse (CMAX), i.e.

$$maxU = UM2 + US2 + UK1 + UO1 = \sum^{m2,s2,k1,o1} (Cmax). \quad (8)$$

Hence, optimal rated speed for maximum yield (Scenario A) will below 100% of maxU as this rarely occurs (when the four considered constituents are in-phase). Two measures of *Vr* are given (% of max U and absolute). The linear regression statistics, and discretised mean *Vr* (as % of maxU) for grouped site current speeds, are given in Table 2 alongside respective performance metrics of the mean trend line fit (RSQ for absolute) and Pearson correlation (RHO) – associated P-value is not shown as all <0.001 at 5% significance. The standard deviation (STD of Table 2) and convergence of shaded area in Fig. 9b show variability in an optimal rated turbine speed (relative to resource), and clear convergence can be seen in the optimal yield scenarios (Scenarios A and A2).

Optimal rated speed (*Vr*) for scenario B (firm power) varied with resource (i.e. current speed climatology at a site); with relative mean *Vr* found to increase with maximum current speed (see Fig. 9 and Table 2) but with a similar amount of variability (STD of Table 2). This increase in scenario B relative rated turbine speed (*Vr* as % of maxU) is likely the significant decrease in sites resolved when increasing maxU (see Fig. 8a) as well as the tendency for a semi-diurnal (Fig. 8b) and dominant M2 amplitude (Fig. 8c) in the tidal dynamics. Furthermore, spatial variability in Scenario B was found when *Vr* (relative to maxU) were grouped into 6 continents - see Table 3 and are shown in Appendix (Figure A3). Therefore, our analysis shows an optimal tidal-stream turbine rated speed (*Vr*) based on firm power supply – spatially varies due to the nature of the tide and the magnitude of the resource.

4. Discussion

Complex analysis involving a large amount of data resulted in a simple set of rules researchers and engineers can use in renewable energy resource assessment:

(1) Tidal-turbine cut-in speed (*Vs*) was found to be ~30% of rated turbine speed (*Vr*) on average;
(2) For a deployment concerned with near-maximum yield aspirations, rated tidal-stream turbine speed (*Vr*) at a given site will be ~87% to 97% of site maximum flow respectively (where max flow is assumed as the sum of current speed amplitude of M2, S2, K1 and O1 constituents: see Ref. [19], with little global variation found;
(3) Deployments concerned with firm, constant power and small amounts of storage, may aim to deploy tidal-stream turbines with much lower rated speeds (~56% of site maximum flow), with spatial variability due to resource (maximum current speed) and the tidal form (F value) – due to the nature of the tide at a given site (see Ref. [19]);
(4) Average values of normalised data from fourteen horizontal axis tidal-stream turbines (Table 1), alongside our estimation of optimal cut-in and rated speed, allows a standardised power curve and device behaviour (Fig. 3) to be implemented in resource and environmental impact assessment, without bias to one specific design (e.g. Ref. [20]) to allow tidal energy resource mapping for future technologies (e.g. Ref. [15]).

Table 3
The linear trend of optimal absolute rated turbine speed ("Trend" Vr in m/s), with each respective linear regression score (RSQ), for three tidal-stream energy scenarios (A, A2, and B) and spatially grouped data by continent, using four major tidal constituents of FES2014 data (latitude <70° and up to 25 km offshore).

region	Scenario:	A (max yield)	A2 (high yield)	B (firm power)
World	RSQ	100%	100%	92%
	Trend	$Vr = 0.97*maxU$	$Vr = 0.87*maxU$	$Vr = 0.56*maxU$
Europe:	RSQ	100%	100%	93%
	Trend	$Vr = 0.96*maxU$	$Vr = 0.85*maxU$	$Vr = 0.46*maxU$
Australasia:	RSQ	100%	100%	91%
	Trend	$Vr = 0.97*maxU$	$Vr = 0.87*maxU$	$Vr = 0.54*maxU$
Asia:	RSQ	100%	100%	93%
	Trend	$Vr = 0.96*maxU$	$Vr = 0.85*maxU$	$Vr = 0.46*maxU$
Africa:	RSQ	99%	99%	91%
	Trend	$Vr = maxU$	$Vr = 0.92*maxU$	$Vr = 0.53*maxU$
North America:	RSQ	100%	99%	95%
	Trend	$Vr = 0.98*maxU$	$Vr = 0.89*maxU$	$Vr = 0.61*maxU$
South America:	RSQ	100%	100%	96%
	Trend	$Vr = 0.99*maxU$	$Vr = 0.89*maxU$	$Vr = 0.74*maxU$

Table 4
Comparison of optimal tidal-stream turbine rated speed (Vr) based on two scenarios (max yield and firm power; scenarios A and B respectively) using tidal harmonic data, giving peak current speed as the sum of the four major constituents (K1,O1,S2,M2), called maxU, as well as the amplitude of current speed for the M2 constituent (Ua), for high and coarse spatial resolution (Res.) model data comparison for the UK region. Comparison metrics: Root Mean Squared Error RMSE) and linear regression score (RSQ) provided alongside scatter and average conversion between resolutions.

	High res. Robins et al. [19] (~1 km spatial resolution)	Coarse res. FES2014 (~7 km resolution)
Scenario A linear trend:	Vr~0.97maxU+0.01	Vr~0.98maxU
Scenario B linear trend:	Vr~0.58*maxU+0.05	Vr~0.56maxU + 0.27
M2 current amplitude comparison:	RMSE = 0.18 m/s (4%) RSQ = 71% Scatter Index = 31% Coarse (Ua) ~ 0.66*high (Ua)	
Maximum current comparison:	RMSE = 0.23 m/s (4%) RSQ = 71% Scatter Index = 28% Coarse res. (maxU) ~ 0.68*high res. (maxU)	

To ensure the result is not affected by the tidal harmonics data, the analysis of the two scenario extremes (maximum yield and firm power: Scenarios A and B) were compared to the result from tidal data at higher resolution: latitudinal resolution of 1/100°(~1 km) instead of 1/16°(~7 km) in the FES2014 global data. The higher resolution tidal data was taken from the Robins et al. [19] hydrodynamic model of a UK domain (14°W to 11°E, and 42°N to 62°N), using the same four tidal constituents (M2, S2, K1 and O1) computed from a 30 day simulation. FES2014 data were interpolated to the Robins et al. [19] computational grid and domain, and *Vr* optimisation (of section 3.3) repeated; the comparison of the optimisation algorithm, using tidal harmonic data from these two spatial resolutions, is shown in Table 4.

To compare sensitivity of turbine optimisation to tidal model data accuracy (Table 4), Root Mean Squared Error (RMSE) and Linear Regression score (RSQ) were estimated assuming the higher resolution data accurate, alongside Scatter Index and the mean downscaling value to convert between model spatial resolutions (e.g. M2 amplitude of coarse data was 66% of the higher resolution model on average). Therefore, the tidal resource data may differ between the two model resolutions (coarse data under-predicting flow speed), but the optimal rated turbine design was found to be constant and independent of tidal flow speed (see Table 4) likely because the relative size of the four tidal constituents, used in this study, slowly spatially vary whilst tidal current magnitude is enhanced by bathymetry – and thus dependant on model spatial resolution.

Indeed, the tidal data sensitivity test (Table 4) showed that although spatially coarse data under-predicted tidal current speeds (both maximum and the main M2 constituent – see Table 4), the optimal rated turbine speed (*Vr as a % of maxU*) was independent of tidal data resolution. Anecdotal verification of optimal turbine rated speed, using the coarse data, can be assessed by comparing our optimal rated speed result to an industry driven solution; for example, the Meygen site (Pentland Firth) has a maximum current speed ~3.5 m/s [25] giving an estimated rated speed (*Vr)* of 2.9 m/s to 3.4 m/s (for A2 and A: high to maximum yield scenarios), which is very close to the 2.65 m/s to 3.05 m/s turbines installed at the site (e.g. Ref. [37]) especially given the extremely coarse global tide data (~7 km spatial resolution).

It is likely that the relative magnitude of the major tidal constituents (i.e. excluding over-tides such as M4), which describe tidal form (F value), has low spatial variability (e.g. Refs. [19,38]; therefore, tidal dynamics (i.e. nature of tide) are resolved in coarse models as spatial variation is small, but tidal current amplitudes are under-predicted because coarse models do not resolve bathymetric features that accelerate tidal currents (see Ref. [15]). Therefore, coarse resolution tidal data can be used to resolve tidal dynamics, but not the magnitude of theoretical tidal-stream energy resource – hence, future resource mapping efforts must be based on high resolution tidal data (also concluded in Ref. [38]). Higher tidal harmonics (such as the combination of M2 and M4, leading to overtides and flood-ebb asymmetry) can have a significant effect on resource assessment [39], and are enhanced by tidal-stream turbine deployments (e.g. Ref. [28]), whilst interaction of array-scale tidal energy developments must be included within resource assessment (e.g. Refs. [18,22]); therefore, we hope the standardised power curve presented here will lead to improved understanding of tidal-stream energy potential.

The approach taken to provide a standardised power curve for use in tidal-stream resource assessment, builds on the work of Hardisty [17] in the application of an idealised tidal-stream power curve, and device technology reviews of Roberts et al. [40] and Zhou et al. [41]. In the technologically mature wind energy industry [42], there is reported convergence in wind turbine cut-in speeds (due to insufficient torque to initiate turbine rotation at wind speeds lower than 3 m/s) and rated speeds (11–17 m/s), although some variability in design depending on local wind conditions [43]. The knowledge of a common power curve in the wind industry has supported mean resource assessment with much research now focusing on finer-scale variability [42,44]. Therefore, our simple set of tidal turbine power curve rules, set out in this paper, would allow improved resource and impact assessments with hydrodynamic models.

Given the deterministic predictability of tidal-stream resource, and the establishment of a standardised and resource-led power curve (presented here), a convergent tidal-stream energy power curve should be the focus of future research to aid resource mapping (e.g. "mhkit"; [45]. If we apply technology development of tidal-stream energy (based on [15]): 1st to 3rd generation sites have peak flow speeds >2.5 m/s, 2 m/s, and 1.5 m/s respectively. Applying the high yield optimisation (Scenario A2) to the global tidal data: 1st generation devices should be considered having rated speeds above 2.2 m/s (*Vs* ~ 0.7 m/s), with 2nd generation rated speed above 1.7 m/s (*Vs* ~0.5 m/s) and 3rd generation rated speed above 1.3 m/s (*Vs* ~0.4 m/s); close to the 0.5 m/s current speed threshold to initiate turbine rotation [32].

Technological learning has led to a reduction in the cost of wind

energy devices [33], and a similar cost reduction is expected for tidal energy [14]. Our analysis confirms tidal turbine rated speed optimisation can be achieved. The inclusion of swept tidal-stream turbine area, alongside economies of scale, practical and socio-economic constraints (e.g. Ref. [13]), would therefore allow for a convergent resource-optimised tidal turbine design and cost assessment. However, future research must resolve uncertainties in array design choice (e.g. Ref. [46]; for example, resolving cost of optimised device resilience (maintenance) and yield, will one turbine be installed throughout a country, region or array?

The predictability of tidal energy, compared to the temporal variability of other non-thermal renewable energy resources (see Ref. [6] and the analysis presented here), indicates the need for develop tools that can perform "whole systems" design of renewable energy systems – where the storage costs and dispatchability of power included in supply-demand analysis (e.g. Refs. [47,48]) as well as resilience and reliability [14]. As power is proportional to the cube of velocity (equation (1)), challenges in competitive costed low-flow tidal turbines are clear (i.e. low yields will likely raise LCOE greatly). However, the potential for low-flow tidal energy devices appears great if we consider the persistence of power density achieved with a Scenario B power curve (gap in power <2 h with the highest Capacity Factor), the cost of storage and resilience in an off-grid energy solution: for example, Large lithium batteries (~$500/kWh [11]) and the use of back-up diesel generators (e.g. Ref. [49]).

Given the prevalence of lower tidal flow sites (e.g. Refs. [15,38]), where turbulence intensity [6] and less mean vertical shear [50] will improve resilience of devices [32], the potential cost of low flow tidal-stream turbines appears an important future step. Applying the conservative "firm power" optimisation (Scenario B) to the global data: 1st generation devices would have a rated speed of ~1.5 m/s (*Vs* ~0.5 m/s), 2nd generation rated speed ~1.2 m/s (*Vs* ~0.4 m/s) and 3rd generation ~0.9 m/s (*Vs* ~ 0.3 m/s). Although all rated speeds in our Scenario B were above the 0.5 m/s threshold, novel turbine designs are will be needed to improve tip-speed-ratios of turbines at low current speed (0.5 m/s or below: [32]). Indeed, our analysis finds ~12.8% of the world's coastlines have maximum current speeds above 1 m/s (resolved in FES2014 up to 25 km offshore and excluding high (>70°) Latitudes), and 3.6% for maxU>1.5 m/s (see Fig. 8 and Appendix Figure A2); however absolute currents speeds are known to be effected by ocean model resolution [15,38] and this number is likely to be much higher. Therefore, higher resolution tidal resource data is needed to perform a full tidal-turbine device optimisation assessment, but the analysis presented here shows a suitable method once such data is available.

Previous research, using high resolution regional models, has shown less energetic flows dominate South East Asia (e.g. Ref. [32]), such Malaysia (current velocities reaching up to 1.2 m/s [51]) and Philippines ("most areas reaching current velocities of 1.4 m/s" [32]). The development of floating tidal-stream devices [52] has unlocked the potential for 2nd and 3rd generation tidal energy sites in the Gulf of California (where peak currents are between 1.0 and 2.4 m/s [53]), and the Kuroshio current (where 1 m/s to 1.5 m/s oceanic currents could be harnessed with floating deep-water, large swept area devices [54]). Indeed, low-flow rated (1.3 m/s to 1.7 m/s) tidal energy kites, with a large swept area, are also being tested and deployed [29,40]. However, there is still a gap in low flow tidal turbines for lower power demand markets and "blue growth economies" [16]. For example, incorporation of tidal energy into offshore aquaculture would require tidal-stream devices capable of operating in <1 m/s flows (see Gentry et al., [59]), and although some bio-optimisation to accelerate tidal currents is possible [30] it may not be required given modest power needs [55]. We therefore, find two tidal-stream turbine markets and designs may be found in the future: (1) larger MegaWatt scale electricity production for grid-connected regions and (2) smaller-scale power systems that provide firm energy for higher value, remote industries and communities.

5. Conclusion

Given the sparsity of published power curves in the literature, and the diverse range of markets tidal energy could benefit, an unbiased power curve characterisation is essential to map tidal-stream energy resource. A standardised tidal-stream power curve was developed so that resource assessment beyond realised technologies can be possible. Our analysis and resource-led optimisation was unaffected by tidal data; finding divergence in rated-speed based on weighting of importance: firm power with low amounts of storage, or high yield with larger storage needs. A general rule for turbine power curve of a horizontal-axis turbine was found: cut-in speed was around 30% of the rated speed; and optimal rated speed (tidal current when peak power converted) was either ~50% or greater than 87% of a site's maximum current speed (based on sum of M2, S2, K1 and O1 harmonic constituents) for firm power or maximum yield respectively - due to the dominance of the major semi-diurnal lunar tidal constituent (M2). This paper demonstrates the "power" of deterministic predictability with tidal energy, and although temporal variability of the tidal resource appears to be captured by current tidal data products, higher resolution data could transform the tidal-stream energy industry by fully mapping the resource. This work also adds to the weight of evidence that a convergent tidal turbine design is needed, and possible, but two tidal-stream turbine types may exist: one for electricity supply to large grid connected communities, and another "lower resource" turbine for remote industry and communities that may have much lower rated speeds.

Declaration of competing interest

I declaration no conflicts of interest.

Acknowledgements

M. Lewis, P. Robins and S. Neill acknowledge the support of SEEC (Smart Efficient Energy Centre) at Bangor University, part-funded by the European Regional Development Fund (ERDF), administered by the Welsh Government. M. Lewis is funded through the EPSRC METRIC fellowship (EP/R034664/1) and wishes to acknowledge Deltares for hosting his research visit in 2019. It is dedicated to M Lewis' late friend, and mentor, Dr. Gerbrant van Vledder. This manuscript was developed during conversations with Dr. D Coles, who helped inform the discussion and future work from this research. This paper was developed during the visit of Dr. S Fredriksson to Bangor University, as part of the PRIMARE SRV grant (Goward-Brown: PI). Dr. Fredriksson wishes to acknowledge supported by the Swedish Energy Agency.

Appendix

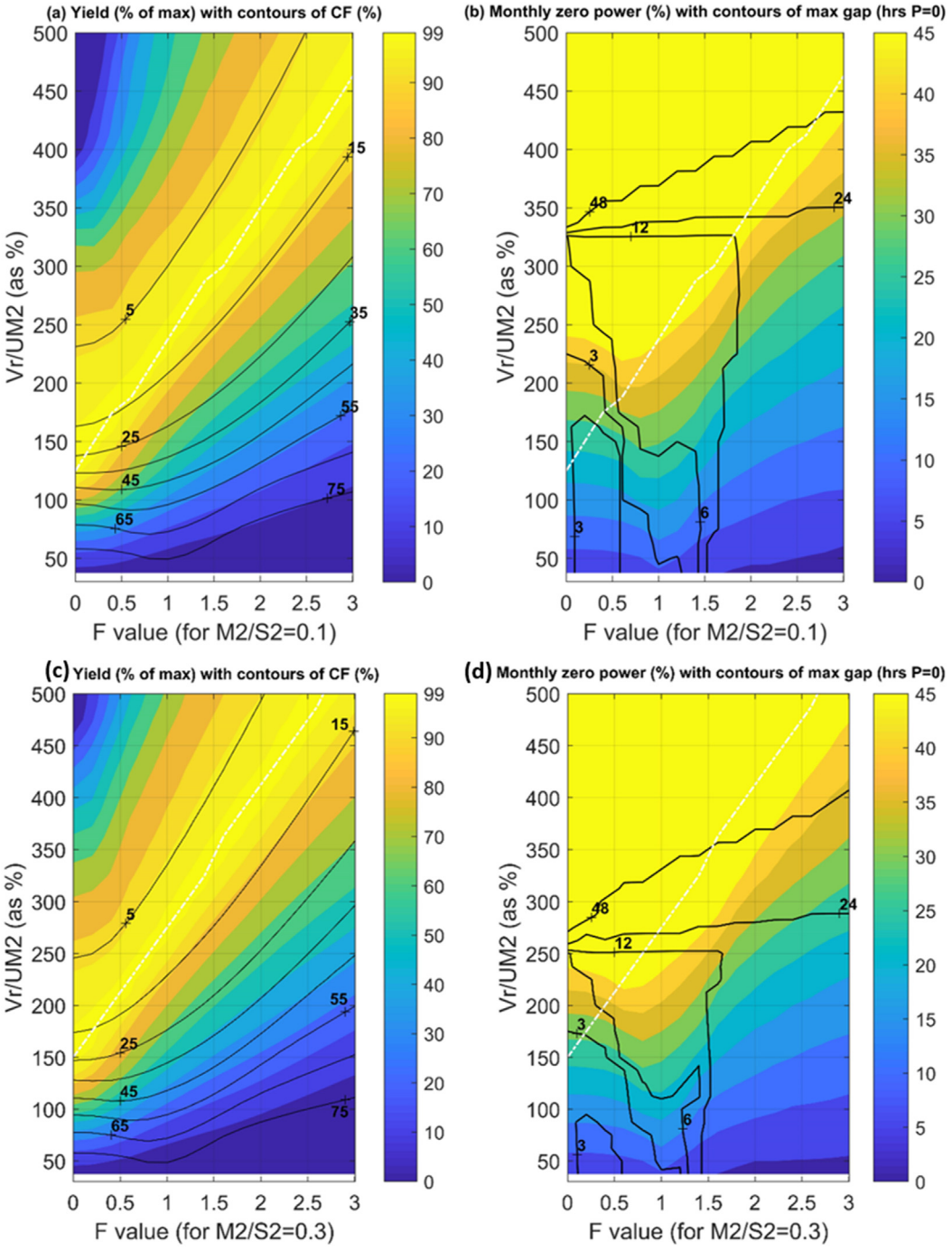

Fig. A1. An example of sensitivity to the tidal-stream turbine optimisation result of Fig. 7, when considering tidal dynamics with different M2/S2 ratios but equal F values. Tide currents harmonic characteristic tidal form (F value), rated turbine speed (relative to M2 current amplitude UM2) and subsequent yield and Capacity Factor (CF) shown in panel a and c; with mean monthly percentage of zero power and maximum period of no power (max gap) in panel b and d.

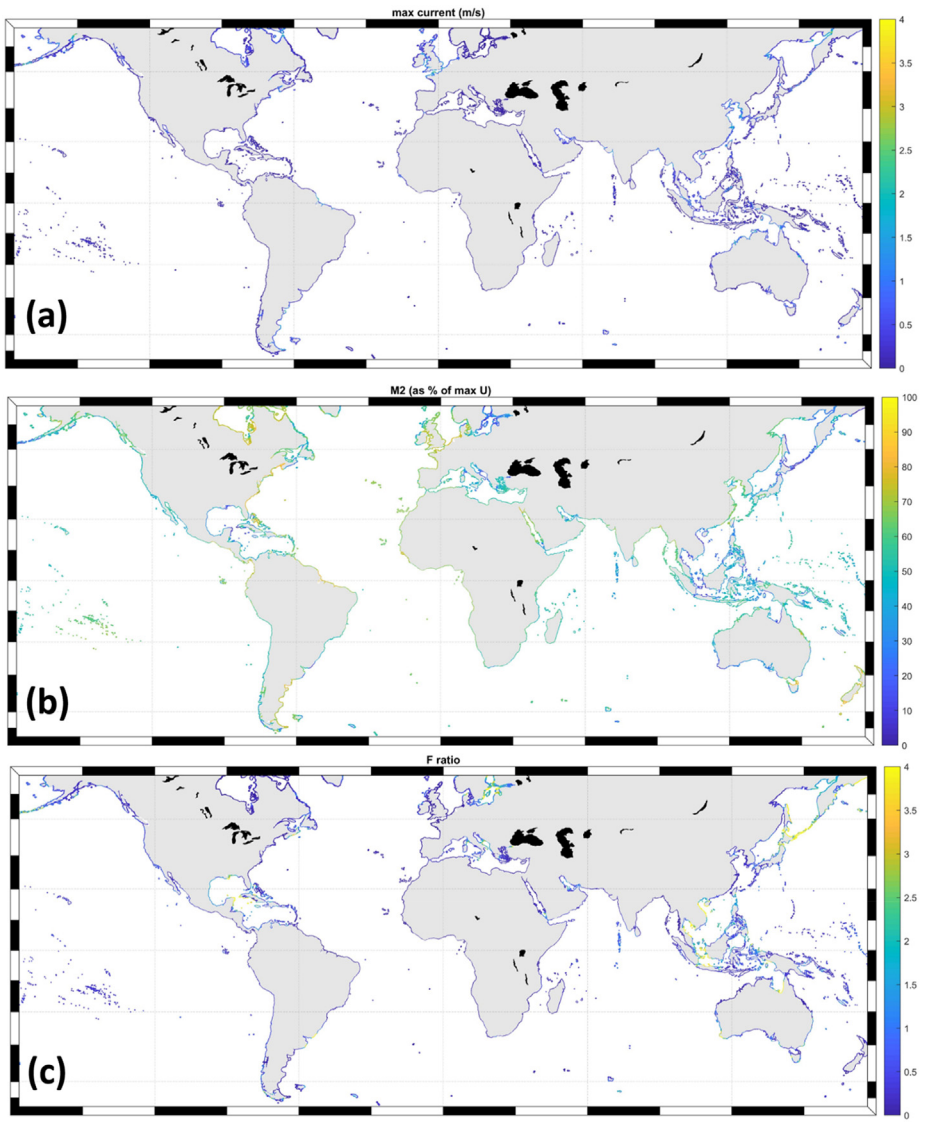

Fig. A2. Global tidal dynamic variability, described as: (a) maximum current speed; (b) percentage of M2 current amplitude compared to maximum current speed; and (c) Tidal form (F-value) using FES2014 data .

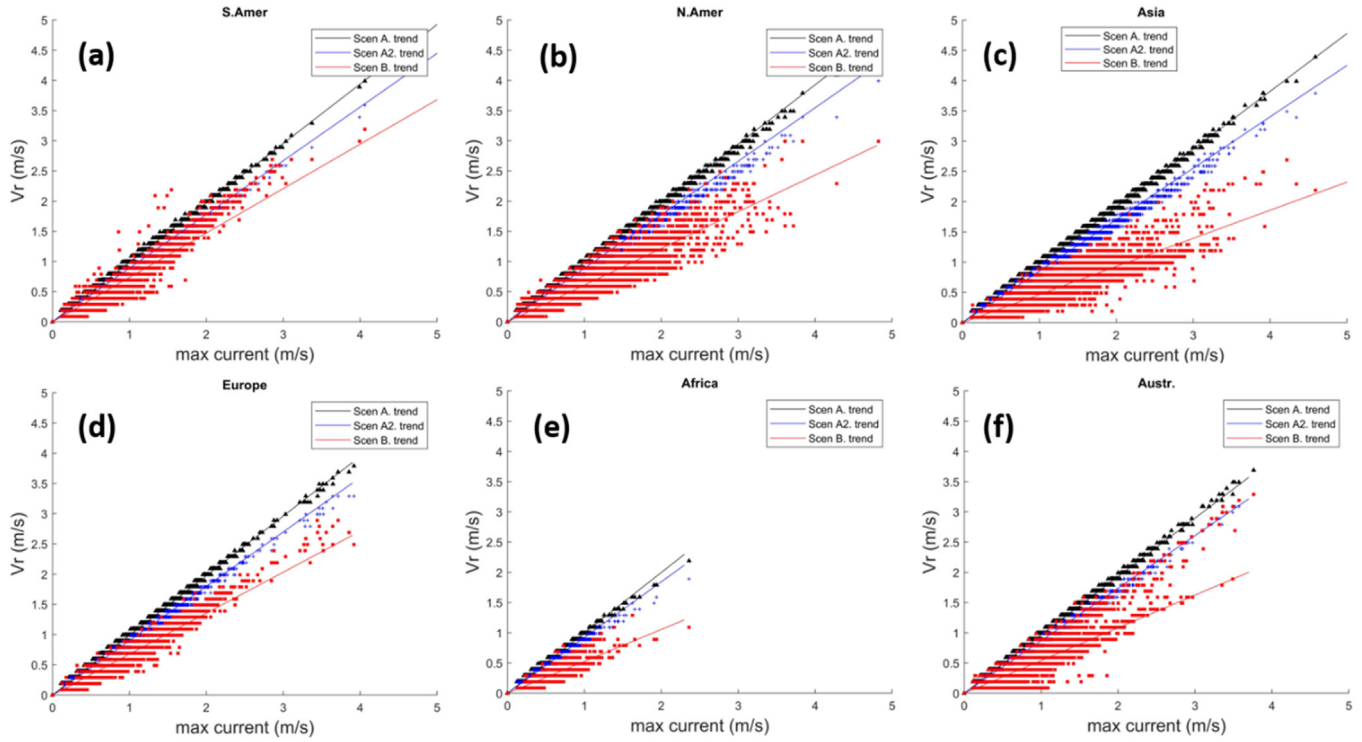

Fig. A3. The optimal rated tidal-stream turbine speed, for three scenarios (a to c for max, high and firm yield respectively), based on FES2014 global data and grouped into the 6 continents: South America (a), North America (b), Asia (c), Europe (d), Africa (e), Australasia (f)..

References

[1] J.S. Tsai, F. Chen, The conceptual design of a tidal power plant in Taiwan, J. Mar. Sci. Eng. 2 (2) (2014) 506–533.
[2] I. Masters, A. Williams, T.N. Croft, M. Togneri, M. Edmunds, E. Zangiabadi, I. Fairley, H. Karunarathna, A comparison of numerical modelling techniques for tidal stream turbine analysis, Energies 8 (8) (2015) 7833–7853.
[3] S.P. Neill, M.R. Hashemi, M.J. Lewis, Tidal energy leasing and tidal phasing, Renew. Energy 85 (2016) 580–587.
[4] A.J. Goward Brown, M. Lewis, B.I. Barton, G. Jeans, S.A. Spall, Investigation of the modulation of the tidal stream resource by ocean currents through a complex tidal channel, J. Mar. Sci. Eng. 7 (10) (2019) 341.
[5] A. Zhang, Y. Sun, W. Yang, H. Huang, Y. Feng, Optimal dispatching of offshore microgrid considering probability prediction of tidal current speed, Energies 12 (17) (2019) 3384.
[6] M. Lewis, J. McNaughton, C. Márquez-Dominguez, G. Todeschini, M. Togneri, I. Masters, M. Allmark, T. Stallard, S. Neill, A. Goward-Brown, P. Robins, Power variability of tidal-stream energy and implications for electricity supply, Energy 183 (2019) 1061–1074.
[7] F.O. Rourke, F. Boyle, A. Reynolds, Marine current energy devices: current status and possible future applications in Ireland, Renew. Sustain. Energy Rev. 14 (3) (2010) 1026–1036.
[8] A. Mason-Jones, D.M. O'Doherty, C.E. Morris, T. O'Doherty, C.B. Byrne, P.W. Prickett, R.I. Grosvenor, I. Owen, S. Tedds, R.J. Poole, Non-dimensional scaling of tidal stream turbines, Energy 44 (1) (2012) 820–829.
[9] A. Mason-Jones, D.M. O'Doherty, C.E. Morris, T. O'Doherty, Influence of a velocity profile & support structure on tidal stream turbine performance, Renew. Energy 52 (2013) 23–30.
[10] G.D. Egbert, R.D. Ray, Estimates of M2 tidal energy dissipation from TOPEX/Poseidon altimeter data, J. Geophys. Res.: Oceans 106 (C10) (2001) 22475–22502.
[11] T. Nielsen, D. McMullin, B. Lenz, D. Gamboa, Toward 100% renewables in the Faroe Islands: wind and energy storage integration, in: 3rd Int. Hybrid Power Systems Workshop, 2018. Tenerife Spain, 8-9 May 2018.
[12] L. Lozano, E.B. Taboada, Demystifying the authentic attributes of electricity-poor populations: the electrification landscape of rural off-grid island communities in the Philippines, Energy Pol. 145 (2020) 111715.
[13] A. Vazquez, G. Iglesias, LCOE (levelised cost of energy) mapping: a new geospatial tool for tidal stream energy, Energy 91 (2015) 192–201.
[14] C.M. Johnstone, D. Pratt, J.A. Clarke, A.D. Grant, A techno-economic analysis of tidal energy technology, Renew. Energy 49 (2013) 101–106.
[15] M. Lewis, S.P. Neill, P.E. Robins, M.R. Hashemi, Resource assessment for future generations of tidal-stream energy arrays, Energy 83 (2015) 403–415.
[16] A. LiVecchi, A. Copping, D. Jenne, A. Gorton, R. Preus, G. Gill, R. Robichaud, R. Green, S. Geerlofs, S. Gore, D. Hume, W. McShane, C. Schmaus, H. Spence, Powering the Blue Economy; Exploring Opportunities for, 2019.
[17] J. Hardisty, The tidal stream power curve: a case study, Energy Power Eng. 4 (3) (2012) 132–136.
[18] R. Vennell, S.W. Funke, S. Draper, C. Stevens, T. Divett, Designing large arrays of tidal turbines: a synthesis and review, Renew. Sustain. Energy Rev. 41 (2015) 454–472.
[19] P.E. Robins, S.P. Neill, M.J. Lewis, S.L. Ward, Characterising the spatial and temporal variability of the tidal-stream energy resource over the northwest European shelf seas, Appl. Energy 147 (2015) 510–522.
[20] I. Fairley, M. Lewis, B. Robertson, M. Hemer, I. Masters, J. Horrillo-Caraballo, H. Karunarathna, D.E. Reeve, A classification system for global wave energy resources based on multivariate clustering, Appl. Energy 262 (2020) 114515.
[21] C. Garrett, P. Cummins, The power potential of tidal currents in channels, Proc R Soc A 461 (2005), 2563e72. [7].
[22] C. Garrett, P. Cummins, The efficiency of a turbine in a tidal channel, J. Fluid Mech. 588 (2007) 243e51.
[23] Z. Yang, T. Wang, A.E. Copping, Modeling tidal stream energy extraction and its effects on transport processes in a tidal channel and bay system using a three-dimensional coastal ocean model, Renew. Energy 50 (2013) 605–613.
[24] R. Vennell, Tuning turbines in a tidal channel, J. Fluid Mech. 663 (2010), https://doi.org/10.1007/s10652-011-9214-3, 253e67.
[25] A.J.G. Brown, S.P. Neill, M.J. Lewis, Tidal energy extraction in three-dimensional ocean models, Renew. Energy 114 (2017) 244–257.
[26] M. Kadiri, R. Ahmadian, B. Bockelmann-Evans, W. Rauen, R. Falconer, A review of the potential water quality impacts of tidal renewable energy systems, Renew. Sustain. Energy Rev. 16 (1) (2012) 329–341.
[27] P.E. Robins, S.P. Neill, M.J. Lewis, Impact of tidal-stream arrays in relation to the natural variability of sedimentary processes, Renew. Energy 72 (2014) 311–321.
[28] S.P. Neill, E.J. Litt, S.J. Couch, A.G. Davies, The impact of tidal stream turbines on large-scale sediment dynamics, Renew. Energy 34 (12) (2009) 2803–2812.
[29] H. Buckland, E. Dolerud, T. Baker, Application of standard tidal performance specification and performance review to a non-standard tidal energy converter, in: European Wave and Tidal Energy Conference (EWTEC), 2015. September 2015. Nantes, France.
[30] F. O'Donncha, S.C. James, E. Ragnoli, Modelling study of the effects of suspended aquaculture installations on tidal stream generation in Cobscook Bay, Renew. Energy 102 (2017) 65–76.
[31] N. Guillou, S.P. Neill, P.E. Robins, Characterising the tidal stream power resource around France using a high-resolution harmonic database, Renew. Energy 123 (2018) 706–718.
[32] J.I. Encarnacion, C. Johnstone, S. Ordonez-Sanchez, Design of a horizontal axis tidal turbine for less energetic current velocity profiles, J. Mar. Sci. Eng. 7 (7)

(2019) 197.
[33] M. Junginger, A. Faaij, W.C. Turkenburg, Cost reduction prospects for offshore wind farms, Wind Eng. 28 (1) (2004) 97–118.
[34] L. Carrere, F. Lyard, M. Cancet, A. Guillot, FES 2014, a New Tidal Model on the Global Ocean with Enhanced Accuracy in Shallow Seas and in the Arctic Region, EGU General Assembly, 2015, p. 5481.
[35] R. Pawlowicz, B. Beardsley, S. Lentz, Classical tidal harmonic analysis including error estimates in MATLAB using T_TIDE, Comput. Geosci. 28 (8) (2002) 929–937.
[36] F.H. Lyard, D.J. Allain, M. Cancet, L. Carrère, N. Picot, FES2014 global ocean tides atlas: design and performances, Ocean Sci. Discuss. (2020) 1–40.
[37] Website 2, Atlantis published turbine characteristics. https://simecatlantis.com/, 2019.
[38] M. Lewis, S. Neill, P. Robins, A. Goward-Brown, A resource assessment to inform second-generation tidal-stream energy device design, in: European Wave and Tidal Energy Conference, 2017, 2017. Cork Ireland.
[39] S.P. Neill, M.R. Hashemi, M.J. Lewis, The role of tidal asymmetry in characterizing the tidal energy resource of Orkney, Renew. Energy 68 (2014) 337–350.
[40] A. Roberts, B. Thomas, P. Sewell, Z. Khan, S. Balmain, J. Gillman, Current tidal power technologies and their suitability for applications in coastal and marine areas, Journal of Ocean Engineering and Marine Energy 2 (2) (2016) 227–245.
[41] Z. Zhou, M. Benbouzid, J.F. Charpentier, F. Scuiller, T. Tang, Developments in large marine current turbine technologies—a review, Renew. Sustain. Energy Rev. 71 (2017) 852–858.
[42] M. Lydia, S.S. Kumar, A.I. Selvakumar, G.E.P. Kumar, A comprehensive review on wind turbine power curve modeling techniques, Renew. Sustain. Energy Rev. 30 (2014) 452–460.
[43] C. Carrillo, A.O. Montaño, J. Cidrás, E. Díaz-Dorado, Review of power curve modelling for wind turbines, Renew. Sustain. Energy Rev. 21 (2013) 572–581.
[44] F. Trivellato, L. Battisti, G. Miori, The ideal power curve of small wind turbines from field data, J. Wind Eng. Ind. Aerod. 107 (2012) 263–273.
[45] Website 4, "mhkit" a toolbox for renewable energy resource assessment. https://mhkit-software.github.io/MHKiT/tidal.html, 2019.
[46] D.S. Coles, L.S. Blunden, A.S. Bahaj, The energy yield potential of a large tidal stream turbine array in the Alderney Race, Philosophical Transactions of the Royal Society A 378 (2178) (2020) 20190502.
[47] A. Stegman, A. De Andres, H. Jeffrey, L. Johanning, S. Bradley, Exploring marine energy potential in the UK using a whole systems modelling approach, Energies 10 (9) (2017) 1251.
[48] D. Al Katsaprakakis, B. Thomsen, I. Dakanali, K. Tzirakis, Faroe Islands: towards 100% RES penetration, Renew. Energy 135 (2019) 473–484.
[49] K. Mala, A. Schläpfer, T. Pryor, Case studies of remote atoll communities in Kiribati, Renew. Energy 34 (2) (2009) 358–361.
[50] M. Lewis, S.P. Neill, P. Robins, M.R. Hashemi, S. Ward, Characteristics of the velocity profile at tidal-stream energy sites, Renew. Energy 114 (2017b) 258–272.
[51] Y.S. Lim, S.L. Koh, Analytical assessments on the potential of harnessing tidal currents for electricity generation in Malaysia, Renew. Energy 35 (2010) 1024–1032.
[52] S.A. Brown, E.J. Ransley, S. Zheng, N. Xie, B. Howey, D.M. Greaves, Development of a fully nonlinear, coupled numerical model for assessment of floating tidal stream concepts, Ocean Eng. 218 (2020) 108253.
[53] C.J. Mejia-Olivares, I.D. Haigh, N.C. Wells, D.S. Coles, M.J. Lewis, S.P. Neill, Tidal-stream energy resource characterization for the Gulf of California, México. Energy 156 (2018) 481–491.
[54] T. Liu, B. Wang, N. Hirose, T. Yamashiro, H. Yamada, High-resolution modeling of the Kuroshio current power south of Japan, J. Ocean Eng. Mar. Energy 4 (2018) 37–55.
[55] Aquatera, Renewable power generation on aquaculture siteS, SARF093, report by Aquatera LtD, 2014, 2014, www.sarf.org.uk.
[56] Website 1, Sabella published turbine characteristics. https://www.sabella.bzh/en, 2019.
[57] B. Polagye, A. Copping, K. Kirkendall, G. Boehlert, S. Walker, M. Wainstein, B. Van Cleve, Environmental Effects of Tidal Energy Development: a Scientific Workshop, University of Washington, Seattle, Seattle, WA, USA, 2010. NMFS F/SPO-116, NOAA.
[58] Website 3, Schottel published turbine characteristics. https://www.schottel.de/schottel-hydro/sit-instream-turbine/, 2019.
[59] R.R. Gentry, H.E. Froehlich, D. Grimm, P. Kareiva, M. Parke, M. Rust, S.D. Gaines, B.S. Halpern, Mapping the global potential for marine aquaculture, Nat. Ecol. Evol. 1 (9) (2017) 1317–1324, https://doi.org/10.1038/s41559-017-0257-9.